Numerical Aspects of Determination of Natural Frequencies of a Power Transmission Line Cable Equipped with In-line Fittings

Hinko Wolf[a,*], Sanja Singer[a], Dragan Pustaić[b], Neven Alujević[a]

[a] *University of Zagreb, Faculty of Mechanical Engineering and Naval Architecture, Ivana Lučića 5, 10000 Zagreb, Croatia*
[b] *retired from University of Zagreb, Faculty of Mechanical Engineering and Naval Architecture, Ivana Lučića 5, 10000 Zagreb, Croatia*

Abstract

In the analysis of Aeolian vibration response of electric power transmission lines, the modified energy balance method (MEBM) is often used. The first and crucial step in applying the MEBM is an accurate determination of the natural frequencies and modes of the system, or in other words, the eigenvalues and eigenvectors of the system matrix. In this paper an efficient numerical procedure that searches for frequency parameters s that make the system matrix $J(s)$ of transmission line cable singular is considered. A realistic case where the cable is equipped with in-line fittings such as Stockbridge vibration dampers and aircraft warning spheres is taken into account. It is shown that the rank of the considered system matrix $J(s)$ is either full, or the full rank minus one. From a numerical point of view, this is an important property of the system matrix since multiple eigenvalues without a full set of eigenvectors, i.e., with Jordan blocks of order greater than 1, are very sensitive to small perturbations. The developed numerical procedure, which is easily parallelizable, consists of the hybrid minimization method paired with the Singular Value Decomposition (SVD) for the detection of the singularity of the matrix. Presented numerical examples illustrate advantages of the numerical procedure proposed.

Keywords: Aeolian vibrations, transmission line, SVD, singularity detection

1. Introduction

Intense vibrations can be observed in electric overhead transmission lines, submarine periscopes, tall chimneys and other similar objects, when certain conditions are fulfilled regarding the interaction of the fluid flow and the dynamics of the structure. For example, if one considers a fluid flowing past a cylinder, a regular pattern of alternating vortices, the so-called von Kármán vortices, can occur. These vortices change between clockwise and counter-clockwise rotation direction and produce harmonically varying lift forces on the cylinder perpendicular to the fluid velocity. If the Reynolds number (Re) spans from 60 to 5000, experimental data confirms that a strong regular vortex shedding appears. Vortex shedding means that vortices are created at the back of the body and detach periodically from either side of the body. If the Reynolds number is equal or greater than 1000, we can write the dimensionless frequency of the vortex shedding, through a Strouhal number (St), approximately as

$$\mathrm{St} = \frac{fD}{v}. \tag{1.1}$$

In this equation, f is the frequency of the vortex shedding, D is the diameter of the cylinder, and v is the velocity perpendicular to the longitudinal axis of the cylinder. Being a fully coupled aero-elastic phenomenon, the mechanism of forming and shedding of von Kármán vortices is rather involved [11, 12, 19, 29]. If the frequency of the vortex shedding coincides with a natural frequency of the structure, intense vibrations of the structure can occur.

*Corresponding author.
Email addresses: hinko.wolf@fsb.hr (Hinko Wolf), sanja.singer@fsb.hr (Sanja Singer), dragan.pustaic@fsb.hr (Dragan Pustaić), neven.alujevic@fsb.hr (Neven Alujević)

Vibrations of overhead transmission lines caused by the shedding of von Kármán vortices usually occur in the frequency range of 10 to 50 Hz for low to moderate winds (1–10 m/s). The first natural frequency of a typical overhead transmission line conductor is of the order of 0.1 Hz. Therefore, the frequency range of 10 to 50 Hz approximately corresponds to the interval from the 100th to the 500th eigenfrequency of the cable. This means that almost certainly the vortex shedding frequency matches a natural frequency of the cable. This regularly causes vibrations of relatively low amplitudes (up to a conductor diameter). However, the cable undergoes a very large number of cycles. This kind of wind induced vibrations with relatively small amplitudes but with prolonged duration is often referred to as Aeolian vibrations [14, 22, 25]. Aeolian vibrations cause damage and even structural failure of the cable due to material fatigue and significantly shorten its lifetime [1, 8].

Extreme fatigue of cable strands occurs at points where motion of the cable is constrained against transverse vibrations. These points are typically suspension clamps, Stockbridge damper clamps, spacer-damper clamps, and aircraft warning sphere clamps. Spans with aircraft warning spheres are prone to intense Aeolian vibrations, especially inside sub-spans in between two adjacent warning spheres. It is often the case that the strains at warning sphere clamps are larger than the corresponding bending strains at the suspension clamps [2, 7, 22] and are beyond the allowed limit [2]. In order to avoid damage of the cable near the warning sphere clamps, attention should be paid to determining the optimal position of Stockbridge dampers near the suspension clamps, as well as near the warning sphere clamps. Because of this, a reliable and numerically efficient procedure for the calculation of bending strains at an arbitrary point in the span is needed.

Aeolian vibrations of overhead transmission lines are in practice most often estimated by using the Energy Balance Method (EBM) [9–11, 17] and the Modified Energy Balance Method using eigenfunctions (MEBM) [12, 26–28]. By applying the EBM, a relatively dense discrete spectrum of natural frequencies of the considered cable is approximated by the continuous spectrum of a semi-infinite one. The energy balance between the power injected into the system through the aerodynamic forces, the power dissipated by the vibration dampers, and the power dissipated by the conductor due to the conductor's self-damping is then carried out for all frequencies of interest. After the average free-field vibration amplitudes are obtained, the bending strains can be determined by using approximate expressions [9]. It must be emphasized that this simple and numerically very efficient method can be applied only if the in-line fittings (e.g., Stockbridge dampers) are spaced near the suspension clamps. If this is not the case, then the MEBM should be used.

MEBM enables determination of the eigenvalues of a cable with in-span fittings (Stockbridge dampers, aircraft warning spheres), and therefore, enables calculation of bending strains at any point in the span. However, the continuous spectrum approximation can no longer be used, and discrete natural frequencies and the corresponding mode shapes of the cable must be determined. As a result, MEBM is numerically a much more demanding procedure than EMB. MEBM requires a sort of optimization procedure to determine the complex frequency parameters that make the system matrix numerically singular. In each step the system matrix is a bit "more singular" (its smallest singular value becomes even smaller) than the matrix in the previous step, i.e., it has a higher condition number. Thus, the first and the very crucial step of applying the MEBM is the accurate determination of the system eigenvalues.

In this paper it is shown that there are certain difficulties in predicting the bending strains in the cable by using MEBM because they considerably depend on the precision of the computed eigenvalues and eigenvectors. The work presented suggests that the procedure of numerical solution of the eigenvalue problem described in [26–28], can be significantly improved. The improvement is deemed necessary for two reasons. First, as shown in this paper, the method described in [26–28] can be insufficiently accurate which may lead to an inaccurate determination of the corresponding bending strains. Second, the procedure described in [26–28] may lead to asymmetric cable modes even though a symmetric structure is considered. This is not a physically possible result.

It should be emphasized that MEBM is an approximate method. Its accuracy, apart from the numerical aspects of the method, significantly depends on the assumptions that are built into the model, as well as on the input data (wind power input and the mechanical characteristics of the cable and the Stockbridge damper) that are generally difficult to estimate.

The mechanism of forming and shedding of von Kármán vortices is a very complex phenomenon. The empirical data on the influence of the wind force on the cable, as well as on the power which in that way enters the system differ significantly from source to source in the available literature [15]. The data on the characteristics of air flows (velocity and direction of the airflow, turbulence in the fluid flow) on any given location are typically unknown [15]. It is also difficult to estimate the mechanical characteristics of the cable (bending stiffness, characteristic bending diameter, and

self-damping) because they depend on many parameters (cable construction, tension force, vibration frequency and amplitudes, and temperature) [5]. Similar to the wind power input, these data vary considerably from source to source in the literature [4].

Dynamic properties of Stockbridge dampers are usually determined in the lab. The force on the damper clamp is measured while the damper clamp is subjected to controlled translational (harmonic) motion [14]. The frequency response function between the velocity amplitude of the damper clamp and the force acting on it is called impedance. However, for a more accurate description of the damper dynamic properties it is necessary to take into account the rotational motion of the clamp, since both motions co-exist in reality. In this case a Stockbridge damper should be characterized by an impedance matrix connecting forces and torques due to translational and rotational motion of the clamp. This approach is very rarely used in practice due to its complexity. Also, in practice it is usually neglected that the Stockbridge damper impedance is a function of both the frequency and the clamp vibration velocity amplitude, e.g., the nonlinearity of the Stockbridge damper is neglected.

In this study it is shown how to solve the problem of the determination of the natural frequencies by using a hybrid optimization algorithm by either singular value decomposition (SVD), or pivoted QR factorization of the given system matrix. The way of forming the system matrix and the energy balance procedure [26–28] are described briefly in Section 2 and Section 5, respectively. A detailed description of some specific and useful properties of the system matrix as well as the procedure of the numerical solution of the eigenvalue problem used in this paper, are given in Section 3 and Section 4. Numerical examples presented in Section 6 illustrate advantages of the numerical procedures developed in this paper.

2. Vibration model of overhead transmission line with in-span fittings

The model of an overhead transmission line cable with Stockbridge vibration dampers and aircraft warning spheres is shown in Fig. 2.1.

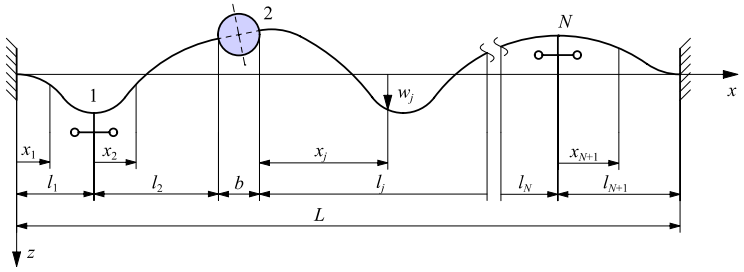

Figure 2.1: Model of an overhead transmission line cable with Stockbridge dampers and aircraft warning spheres.

Overhead transmission line cables are often modeled as beams with bending stiffness EI and tensile forces T at the ends [6, 10, 11]. Transverse vibrations of each sub-span can be described by a non-homogeneous, non-linear partial differential equation of the fourth order (primes denote the differentiation with respect to the space coordinate x, while dots denote the differentiation with respect to the time t)

$$EI\, w_j''''(x_j,t) - T w_j''(x_j,t) + \rho A\, \ddot{w}_j(x_j,t) = q(x_j,t) + d_K(w_j,\dot{w}_j,t), \tag{2.1}$$

where w_j is the transverse vertical displacement of the cable at a location x_j at time t, EI is the cable bending stiffness, T is the cable tension force, ρA is the cable mass per unit length, $q(x_j,t)$ is the wind force imparted on the cable due to von Kármán vortex shedding, and $d_K(w_j,\dot{w}_j,t)$ is the member representing the cable self-damping.

The transverse string vibration model is also often used since the bending stiffness of the cable is small and its influence on the natural frequencies in the frequency range of interest (10–50 Hz) can be ignored [6, 9–11]. In such a case, vibrations are described using the following non-homogeneous non-linear partial differential equation of the second order:

$$-T w_j''(x_j,t) + \rho A\, \ddot{w}_j(x_j,t) = q(x_j,t) + d_K(w_j,\dot{w}_j,t). \tag{2.2}$$

By omitting the forcing terms in Eqn. (2.2) for each sub-span j, $j = 1, \ldots, N+1$, a set of homogeneous linear partial differential equations, that describe free undamped vibrations of the cable are obtained

$$-Tw_j''(x_j,t) + \rho A \ddot{w}_j(x_j,t) = 0, \quad j = 1, \ldots, N+1. \tag{2.3}$$

The solution of Eqn. (2.3) can be written as

$$w_j(x_j,t) = \mathrm{Re}\left(W_j(x_j)e^{st}\right), \qquad W_j(x_j) = A_j e^{sx_j/c} + B_j e^{-sx_j/c}, \quad c = \sqrt{\frac{T}{\rho A}}, \tag{2.4}$$

where c is the wave velocity, A_j and B_j are the integration constants for the vibrations of the jth subspan and

$$s = -\delta + i\omega \tag{2.5}$$

is a complex frequency parameter (imaginary part represents a circular frequency and real part represents a decay coefficient). From the boundary conditions at the left and right suspension clamps i.e., $w_1(0,t) = 0$ and $w_{N+1}(\ell_{N+1},t) = 0$, one obtains

$$A_1 + B_1 = 0, \qquad A_{N+1}e^{k_{N+1}} + B_{N+1}e^{-k_{N+1}} = 0, \tag{2.6}$$

where

$$k_j := k_j(s) = \frac{s\ell_j}{c}, \quad j = 1, \ldots, N+1. \tag{2.7}$$

At the points of attachment of the Stockbridge dampers and the warning spheres the displacement compatibility conditions and force equilibrium equations must be met. As it is shown in [27], the displacement compatibility condition and force equilibrium equation at Stockbridge damper clamp is

$$w_j(\ell_j,t) = w_{j+1}(0,t), \qquad T\left(w_{j+1}'(0,t) - w_j'(\ell_j,t)\right) = F_{Dj}(t), \tag{2.8}$$

where $F_{Dj}(t)$ is the damper force that can be expressed as

$$F_{Dj}(t) = \mathrm{Re}\left(\widehat{F}_{Dj}e^{st}\right) = \mathrm{Re}\left(Z_{Dj}\dot{w}_j(x_{Dj},t)\right), \tag{2.9}$$

where Z_{Dj} is a complex impedance of the jth Stockbridge damper, $\dot{w}_j(x_{Dj},t)$ is a complex velocity of the jth Stockbridge damper clamp and $\widehat{F}_{Dj}$ is a complex amplitude of the damper force. If z_j is defined by $z_j := z_j(s) = cZ_{D_j}(s)/T$, from Eqns. (2.4), (2.8) and (2.9), we have

$$\begin{aligned} A_j e^{k_j} + B_j e^{-k_j} - A_{j+1} - B_{j+1} &= 0, \\ A_j e^{k_j} + B_j e^{-k_j} - A_{j+1}(z_j - 1) - B_{j+1}(z_j + 1) &= 0. \end{aligned} \tag{2.10}$$

Force equilibrium equations at warning spheres clamps are as it is shown in [27]

$$\widehat{F}_{j1} = T\left(w_j'(\ell_j) - \frac{w_{j+1}(0) - w_j(\ell_j)}{b}\right), \qquad \widehat{F}_{j2} = T\left(\frac{w_{j+1}(0) - w_j(\ell_j)}{b} - w_{j+1}'(0)\right). \tag{2.11}$$

$\widehat{F}_{j1}$ and $\widehat{F}_{j2}$ are complex amplitudes of the forces at the left and the right warning sphere claps respectively, that can also be expressed as

$$\begin{bmatrix} \widehat{F}_{j1} \\ \widehat{F}_{j2} \end{bmatrix} = \begin{bmatrix} Z_{11} & Z_{12} \\ Z_{21} & Z_{22} \end{bmatrix} \begin{bmatrix} \widehat{\dot{w}}_j(\ell_j) \\ \widehat{\dot{w}}_{j+1}(0) \end{bmatrix}, \tag{2.12}$$

where

$$Z_{11} = Z_{22} = i\Omega\left(\frac{m}{4} + \frac{J_C}{b^2}\right), \qquad Z_{12} = Z_{21} = i\Omega\left(\frac{m}{4} - \frac{J_C}{b^2}\right), \tag{2.13}$$

are imaginary impedance matrix elements of the warning sphere which is modeled as a rigid body. $\widehat{\dot{w}}_j(\ell_j)$ and $\widehat{\dot{w}}_{j+1}(0)$ are complex amplitudes of the velocities at the left and right warning sphere clamps, m is the mass of the warning sphere, J_C is the mass moment of inertia of the warning sphere and b is the distance between the clamps.

From Eqns. (2.4) and (2.11)–(2.13) we obtain $s = 0$, or

$$\begin{aligned}\left(-\frac{T}{c} - Z_{11}\right)e^{k_j}A_j + \left(\frac{T}{c} - Z_{11}\right)e^{-k_j}B_j - Z_{12}(A_{j+1} + B_{j+1}) = 0,\\ Z_{21}\left(e^{k_j}A_j + e^{-k_j}B_j\right) + \left(\frac{T}{c} - Z_{22}\right)A_{j+1} + \left(-\frac{T}{c} - Z_{22}\right)B_{j+1} = 0.\end{aligned} \tag{2.14}$$

Using Eqn. (2.6) obtained from boundary conditions at the left and right suspension clamps, Eqn. (2.10) obtained from the displacement compatibility condition and the force equilibrium equation at the Stockbridge damper clamp, and Eqn. (2.14) obtained from the force equilibrium equations at the warning spheres clamps, we have a homogeneous system of $2(N + 1)$ algebraic equations with $2(N + 1)$ unknowns A_j, B_j, $j = 1, \ldots, N + 1$, that can be written as

$$J(s)\, a = 0, \quad a = [A_1, B_1, \ldots, A_{N+1}, B_{N+1}]^T. \tag{2.15}$$

Matrix $J(s)$ is referred to as the system matrix since it is a function of the system parameters. Note that Eqn. (2.15) can be seen either as a linear system equation or as an eigenvalue problem, where $a \neq 0$ is the eigenvector for the eigenvalue 0. Since we are interested only in a nontrivial a, $J(s)$ must be singular.

3. Properties of the system matrix $J(s)$

Since the matrix $J(s)$ in Eqn. (2.15) is structured, it has some interesting properties. First, we note that a change of the parameter s can only reduce the rank of $J(s)$ by one. Typically, if the eigenvalues are multiple, their computation is slower than the computation of distinct eigenvalues. In some cases, for example, the inverse iteration method will not converge if two or more eigenvalues have the same distance to the chosen shift.

Theorem 3.1. *The rank of the matrix $J(s)$ from Eqn.* (2.15) *is either* $2N + 2$*, or* $2N + 1$.

Proof. The matrix $J(s)$ from Eqn. (2.15) can be written as a block matrix

$$J(s) = \begin{bmatrix} L & & & & & \\ E_1 & F_1 & & & & \\ & E_2 & F_2 & & & \\ & & \ddots & \ddots & & \\ & & & E_N & F_N & \\ & & & & D \end{bmatrix}, \tag{3.1}$$

where

$$L = \begin{bmatrix} 1 & 1 \end{bmatrix}, \qquad E_j = \begin{bmatrix} e^{k_j} & e^{-k_j} \\ e^{k_j} & -e^{-k_j} \end{bmatrix}, \qquad D = \begin{bmatrix} e^{k_{N+1}} & e^{-k_{N+1}} \end{bmatrix}, \qquad F_j = \begin{bmatrix} -1 & -1 \\ z_j - 1 & z_j + 1 \end{bmatrix}, \qquad j = 1, \ldots, N. \tag{3.2}$$

The rank of $J(s)$ is unchanged if the columns and/or rows of are swapped. This also holds if a multiple of a row (column) is added to another row (column). Therefore, if the first block-column (the first two columns) of $J(s)$ is moved to the end of the matrix, and then the first row is moved after the current last row, the rank of the obtained $J^{(1)}(s)$,

$$J^{(1)}(s) = \begin{bmatrix} F_1 & & & & & E_1 \\ E_2 & F_2 & & & & \\ & \ddots & \ddots & & & \\ & & E_N & F_N & & \\ & & & D & & \\ & & & & L & \end{bmatrix}, \tag{3.3}$$

remains the same. By subtraction of the last column from the penultimate one, only the block matrices E_1 and L are changed, such that the new submatrices on these positions are

$$E_1' = \begin{bmatrix} e^{k_1} - e^{-k_1} & e^{-k_1} \\ e^{k_1} + e^{-k_1} & -e^{-k_1} \end{bmatrix}, \quad L' = \begin{bmatrix} 0 & 1 \end{bmatrix}. \tag{3.4}$$

Finally, if the last row is multiplied by $-e^{-k_1}$ and added to the first row, and then multiplied by e^{-k_1} and added to the second row, only the elements of E_1' are changed. Instead of E_1' we have

$$E_1'' = \begin{bmatrix} e^{k_1} - e^{-k_1} & 0 \\ e^{k_1} + e^{-k_1} & 0 \end{bmatrix}. \tag{3.5}$$

By defining,

$$E_{N+1} = \begin{bmatrix} D \\ 0 \end{bmatrix} = \begin{bmatrix} e^{k_{N+1}} & e^{-k_{N+1}} \\ 0 & 0 \end{bmatrix}, \qquad F_{N+1} = \begin{bmatrix} 0 \\ L' \end{bmatrix} = \begin{bmatrix} 0 & 0 \\ 0 & 1 \end{bmatrix}, \tag{3.6}$$

matrix $J^{(2)}(s)$, obtained by transformations written in Eqns. (3.3)–(3.5), has the same rank as $J(s)$. By using Eqn. (3.6), matrix $J^{(2)}(s)$ can be written as

$$J^{(2)}(s) = \begin{bmatrix} F_1 & & & & & E_1'' \\ E_2 & F_2 & & & & \\ & \ddots & \ddots & & & \\ & & E_N & F_N & & \\ & & & E_{N+1} & F_{N+1} & \end{bmatrix}. \tag{3.7}$$

Now it can be seen that all the matrices F_j are nonsingular since $\det(F_j) = -2$, for $j = 1, \ldots, N$. Now, our goal is to transform $J^{(2)}(s)$ to become a block upper-triangular matrix. By multiplication of the first block-row by $-E_2F_1^{-1}$ and addition to the second block-row, we obtain

$$J^{(3)}(s) = \begin{bmatrix} F_1 & & & & & E_1'' \\ 0 & F_2 & & & & -E_2F_1^{-1}E_1'' \\ & E_3 & \ddots & & & \\ & & \ddots & F_N & & \\ & & & E_{N+1} & F_{N+1} & \end{bmatrix}. \tag{3.8}$$

The same procedure repeated on the rest of the block-rows, i.e., multiplication of the second block-row by $-E_3F_2^{-1}$ and addition to the third block-row, ..., and finally, multiplication of the penultimate block-row by $-E_{N+1}F_N^{-1}$ and addition to the last block-row, gives

$$J^{(N+2)}(s) = \begin{bmatrix} F_1 & & & & E_1'' \\ & F_2 & & & -G_2E_1'' \\ & & \ddots & & \vdots \\ & & & F_N & (-1)^{N-1}G_NE_1'' \\ & & & & F_{N+1} + (-1)^N G_{N+1}E_1'' \end{bmatrix}, \tag{3.9}$$

where

$$G_j = E_jF_{j-1}^{-1} \cdots E_2F_1^{-1}, \quad j = 2, \ldots, N+1. \tag{3.10}$$

Since $J^{(N+2)}(s)$ is a block-triangular matrix, it is singular if and only if its diagonal blocks are singular. Since all F_j, $j = 1, \ldots, N$ are nonsingular, the only block in $J^{(N+2)}(s)$ that can be singular is the last block. Therefore, we are looking for a parameter s that makes the 2×2 matrix F_{N+1}',

$$F_{N+1}' = F_{N+1} + (-1)^N E_{N+1}F_N^{-1} \cdots E_2F_1^{-1}E_1'', \tag{3.11}$$

singular. If we use the shapes of F_{N+1}, and E_{N+1} from Eqn. (3.6) and the shape of E_1'' from Eqn. (3.5), then F_{N+1}' from Eqn. (3.11) has the following form

$$F_{N+1}' = \begin{bmatrix} 0 & 0 \\ 0 & 1 \end{bmatrix} + (-1)^N E_{N+1}F_N^{-1} \cdots E_2F_1^{-1}E_1'' = \begin{bmatrix} 0 & 0 \\ 0 & 1 \end{bmatrix} + (-1)^N \begin{bmatrix} e^{k_{N+1}} & e^{-k_{N+1}} \\ 0 & 0 \end{bmatrix} \cdot F_N^{-1} \cdots E_2F_1^{-1} \begin{bmatrix} e^{k_1} - e^{-k_1} & 0 \\ e^{k_1} + e^{-k_1} & 0 \end{bmatrix}. \tag{3.12}$$

Therefore F'_{N+1} is upper triangular, and

$$F'_{N+1} = \begin{bmatrix} f'_{11} & 0 \\ 0 & 1 \end{bmatrix}. \tag{3.13}$$

The element f'_{11} in F'_{N+1}, determines the rank of F'_{N+1}, and subsequently the rank of $J(s)$, and thus

$$\operatorname{rank}(J(s)) = \begin{cases} 2N+1, & \text{if } f'_{11} = 0, \\ 2N+2, & \text{otherwise,} \end{cases} \tag{3.14}$$

which completes the proof. □

For moderate sizes of N, symbolic software could be used to solve the equation $f'_{11}(s) = 0$. The final solution of the problem is a linear combination of the exponential functions, and therefore could be inaccurate if the sum is a small number compared to the terms in the summation.

4. Numerical solution of the eigenvalue problem

Various algorithms for the solution of the problem in Eqn. (2.15) are described in Refs. [26–28]. They concluded that the determinant search method

$$\det(J(s)) = 0 \tag{4.1}$$

is not applicable.

In the following example it is illustrated why the computation of the determinant is not the method of choice to determine singularity. Suppose that matrix $J(s)$ is singular, of order 70, with 69 eigenvalues equal to 10. Every stable numerical algorithm, during the computation, makes small absolute errors in computed eigenvalues. In our example, if all the eigenvalues are computed as

$$\tilde{\lambda}_j = \lambda_j \pm \varepsilon_j, \quad j = 1, \ldots 70, \tag{4.2}$$

where $|\varepsilon_j|$ is a small number, for example, $|\varepsilon_j| \leq 10^{-14}$, then

$$|\det(J(s))| = |\varepsilon_1| \prod_{j=1}^{69} (10 \pm \varepsilon_j) \approx 10^{-14} \cdot 10^{69} = 10^{55} \gg 0, \tag{4.3}$$

which is far away from zero.

In Ref. [28] Hagedorn and Verma give an alternate method for the solution of Eqn. (2.15), that first transforms homogeneous system to nonhomogeneous (Nonhomogeneous System Solution method, or NSS for short), and then solves the linear system by the Gaussian elimination. However, since the system matrix in each step is more singular than the matrix in the previous step, its condition number $\kappa(A)$,

$$\kappa(A) = \|A\| \, \|A^{-1}\|, \tag{4.4}$$

becomes higher. As a result, the solution of the linear system can be very inaccurate. This is illustrated next. Suppose that two linear systems

$$Ax = b \tag{4.5}$$

and

$$(A + \Delta A)(x + \Delta x) = b + \Delta b, \tag{4.6}$$

where $\|\Delta A\| \leq \varepsilon \|A\|$ and $\|\Delta b\| \leq \varepsilon \|b\|$ are solved. Here $\|\ \|$ denotes any operator vector norm. If the condition number satisfy that $\varepsilon\kappa(A) < 1$ then classical normwise perturbation gives (see, for example [13, Theorem 7.2])

$$\|\Delta x\| \leq \frac{\varepsilon}{1 - \varepsilon\kappa(A)} \left(\|A^{-1}\| \, \|b\| + \kappa(A) \|x\| \right) \leq \frac{2\varepsilon\kappa(A)}{1 - \varepsilon\kappa(A)} \|x\|. \tag{4.7}$$

As we have already noticed, Eqn. (4.1) is only a consequence of the fact that the system matrix $J(s)$ is singular. It is possible to use other methods to determine whether a matrix is singular or not. These include the QR factorization

with column pivoting and the singular value decomposition (SVD). Since the QR factorization is not an iterative process, the former method should be faster (in the case of sequential computation) than the latter, especially for the large matrices. If the matrix is nearly singular, the latter method should be more stable than the former, and easily parallelizable (essential for large matrices) if the SVD is computed by a Jacobi-type method (see, for example, [21, 23, 24].

The QR factorization with column pivoting (at step k of the algorithm, pivoting strategy puts the column with the largest norm as the first column of the temporary submatrix $A(k : 2N+2, k : 2N+2)$ of A) factorizes a complex matrix A such that $A = QRP$, where Q is unitary, R is upper triangular, and P is a permutation matrix. If the QR factorization is performed with column pivoting, only the last element, $R_{\min} := R_{2N+2,2N+2}$, on the diagonal of R should be checked for singularity. Due to pivoting, for the diagonal elements of R, it holds

$$R_{jj}^2 \geq \sum_{l=j}^{k} |R_{lk}^2| \geq R_{kk}^2, \quad k > j. \tag{4.8}$$

In the singular value decomposition method a matrix $A \in \mathbb{C}^{m\times n}$, $m \geq n$ (if $m < n$ then the SVD of A^* is computed) into a product $A = U\Sigma V^*$, where $U \in \mathbb{C}^{m\times m}$ and $V \in \mathbb{C}^{n\times n}$ are unitary matrices, and $\Sigma \in \mathbb{R}^{m\times n}$ such that

$$\Sigma = \begin{bmatrix} \Sigma_{n\times n} \\ 0 \end{bmatrix}, \qquad \Sigma_{n\times n} = \operatorname{diag}(\sigma_1, \sigma_2, \ldots, \sigma_n), \qquad \sigma_1 \geq \sigma_2 \geq \cdots \geq \sigma_n \geq 0. \tag{4.9}$$

Therefore, if the SVD is used, only the minimal singular value, $\sigma_{\min} := \sigma_n$ has to be checked to determine whether the given matrix is singular.

We have tested both methods in our programs. The methods are almost equally fast, but the "surface" $\sigma_{\min}(J(s))$, as in Fig. 4.1, is much smoother than the "surface" $R_{\min}(J(s))$ in the pivoted QR factorization of $J(s)$. Therefore, the method of choice for the detection of singularity is the SVD.

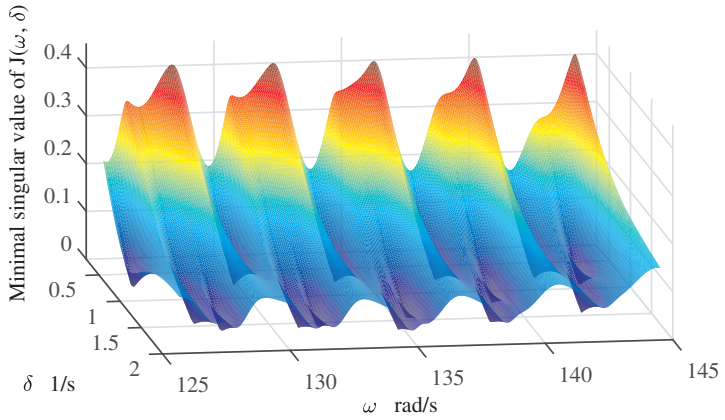

Figure 4.1: Minimal singular value of $J(\omega, \delta)$.

Note that the minimal singular value of J in Fig. 4.1, as well as, in Figs. 4.3, 4.4 and 6.6 is dimensionless.

4.1. Numerical determination of singularity

Our approach also requires the initial values of s from Eqn. (2.5), i.e., ω and δ that are sufficiently close to the parameters that make $J(s) := J(\omega, \delta)$ singular. If the initial values of ω and δ are not close enough, the optimization procedure may not succeed in finding parameters ω_0 and δ_0 such that $J(\omega_0, \delta_0)$ is singular. Fig. 4.1 shows the minimal singular values of $J(\omega, \delta)$ as the real function of two independent variables, ω and δ, for $125 \leq \omega \leq 145$ rad/s and $0 \leq \delta \leq 2$ 1/s (span with aircraft warning spheres and Stockbridge dampers shown in Fig. 4.2).

In order to increase the probability of determining the most of the parameters that make $J(\omega, \delta)$ singular, the initial values ω_i and δ_i are determined by searching the area $\omega_{\min} \leq \omega \leq \omega_{\max}$ with a certain increment $\Delta\omega$. For each of the

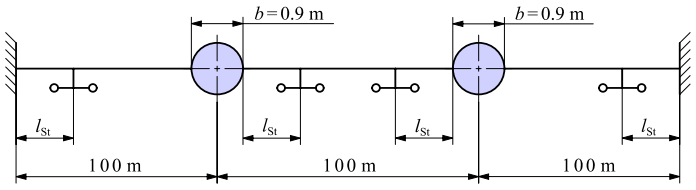

Figure 4.2: Span with 4 Stockbridge dampers and 2 warning spheres.

considered values ω, one varies δ within the area $0 \leq \delta \leq \delta_{\max}$, with some increment $\Delta\delta$. Fig. 4.3 shows the minimal singular value of function $J(\omega, \delta)$ for $\omega = 135.3715$ rad/s ($f = 21.545$ Hz) as a function of δ. For each considered value of ω one determines the value $\delta'(\omega)$ so that function $\sigma_{\min}(J(\omega, \delta'))$ has a local minimum.

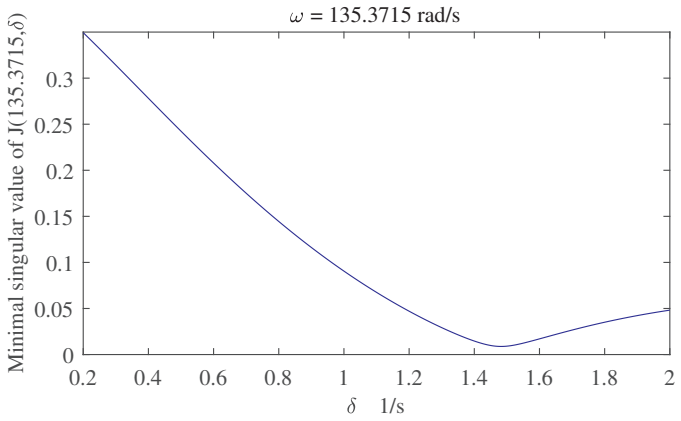

Figure 4.3: $J(135.3715, \delta)$ as a function of δ.

Fig. 4.4 shows the function $\sigma_{\min}(J(\omega, \delta'))$ obtained in this way. Values ω_i for which $\sigma_{\min}(J(\omega, \delta'))$ has local minima (together with the corresponding values δ_i), are the initial values in the process of seeking $\sigma_{\min}(J(\omega_0, \delta_0)) = 0$. The values of increments $\Delta\omega$ and $\Delta\delta$, as well as $\delta_{\max}$, required for obtaining the system eigenvalues, depend on the mechanical properties of the system (cable tensile force, cable mass per unit length, span length, impedance of the warning spheres and Stockbridge dampers as well as their positions inside the span).

It may happen that for certain combinations of initial conditions and/or inadequate choice of $\Delta\omega$, $\Delta\delta$ and $\delta_{\max}$ the minimization process is "trapped" in one of the local minima which do not make $J(\omega, \delta)$ singular. Therefore it is recommended to verify whether $\sigma_{\min}(J(\omega, \delta)) \approx 0$.

If $\sigma_{\min}(J(\omega, \delta))$ is sufficiently close to 0, the parameters ω_0 and δ_0 are accepted as parameters that make $J(\omega, \delta)$ (nearly) singular. Otherwise, ω_0 and δ_0 are omitted from the set of parameters that make $J(\omega, \delta)$ singular.

Now suppose that the initial $s' = -\delta' + i\omega'$ is given. First, we check whether $J(s')$ is singular up to a working precision—if it is, then $s_0 = s'$, and the computation process is already done.

We expect that the starting matrix $J(s'_0) := J(s')$ is nearly singular, and the next choice of s', namely, s'_1 is such that $J(s'_1)$ is closer to a singular matrix than $J(s'_0)$. Choice of s'_1 is a constrained optimization problem (constraints keep s'_k in the domain such that $\omega_{\min} \leq \omega_k \leq \omega_{\max}$, and $\delta_k \geq 0$).

4.2. Optimization methods

There are many available (constrained) optimization methods that can determine s_0. For our purposes, it is sufficient to use an optimization method with a penalizing term that prevents the violation of the barrier $\omega_{\min} \leq \omega_k \leq \omega_{\max}$ and $\delta_k \geq 0$.

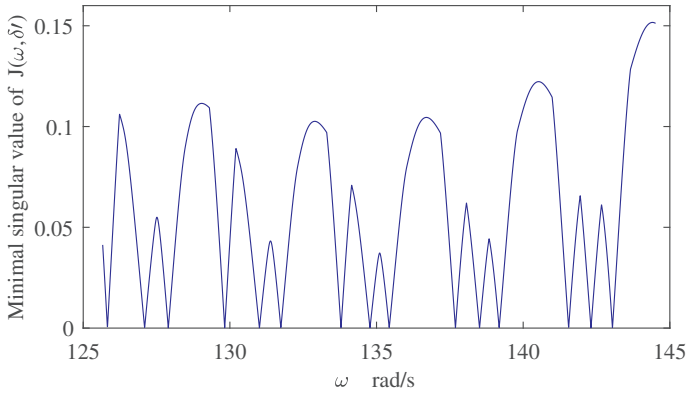

Figure 4.4: Function $\sigma_{\min}(J(\omega, \delta'))$.

In both cases, no matter whether the minimal singular value $\sigma_{\min}$, or the element $R_{\min}$ in the pivoted QR factorization is sought for, we are trying to find s_0 that will minimize the values $\sigma_{\min}(s)$, or $|R_{\min}(s)|$. The easiest way to accomplish this is to use the nonlinear method of least squares, for example, the Levenberg–Marquardt method (see [16, 18]), that minimizes squares of $\sigma_{\min}(s)$, or $|R_{\min}(s)|$. If for some s, $\sigma_{\min}(s) \approx 10^{-8}$, then $(\sigma_{\min}(s))^2 \approx 10^{-16}$, and all the neighboring values $(\sigma_{\min}(s + \Delta s))^2 \approx 10^{-16}$ will have the same order of magnitude. Therefore any optimization method that uses squared values of the errors to determine s_0, can give $\sigma_{\min}(s)$ accurate only on 8 decimal digits. At this point, we switch to an optimization method, such as the Nelder–Mead direct search method (see [20]), that uses absolute values of errors only. The value s'_k is accepted as parameter s_0 when the computed minimal singular value is less or equal to 10^{-14}. Otherwise, some unwanted effects can happen in the numerical simulation of cable behavior.

To check whether the optimization method fails to find parameter s_0 with the prescribed accuracy, we introduced the quantity "cleaning parameter" `cln_fct` usually set in the range 10^{-10}–10^{-14}. If the minimal singular value is less or equal than `cln_fct`, then the matrix is numerically singular. The procedure that finds s'_k such that $\sigma_{\min}(s'_k) \approx 0$, by the hybrid two-stage optimization process that consists of the Levenberg–Marquardt and the Nelder–Mead method, together with the check that $\sigma_{\min}(s'_k) \leq$ `cln_fct` is called the `SVD_OPT`.

When the final s'_k is computed, it is straightforward to compute the eigenvector of $J(s'_k)$, for example, by a single step of the QR algorithm (without a shift), or by the inverse iteration, that corresponds to the eigenvalue closest to 0.

Finally, note that the whole problem of finding parameters s that make $J(s)$ singular is perfectly parallelizable by the division of the natural domain $\omega_{\min} \leq \omega_k \leq \omega_{\max}$, $\delta_k \geq 0$ into the suitable rectangular domains, which can be searched independently.

5. Modified Energy Balance Method

After the complex eigenmodes are determined, one can formulate the energy balance by equating the wind power input over the whole span to the power dissipated in all Stockbridge dampers and the power dissipated in the cable due to the cable self-damping [12, 26–28], as follows

$$\sum_{j=1}^{N+1} P_{W_j} = \sum_{j=1}^{N} P_{D_j} + \sum_{j=1}^{N+1} P_{C_j}, \tag{5.1}$$

where P_{W_j} is the power of aerodynamic forces brought into the jth subspan, P_{D_j} is the power dissipated by the jth Stockbridge damper, while P_{C_j} is the power dissipated inside the jth subspan due to cable self-damping. The vibration amplitude of the cable can be determined using the non-linear algebraic Eqn. (5.1) for any given resonance frequency.

Empirically obtained equations are applied to determine the maximum power brought into the system by aerodynamic forces due to a stationary laminar air flow. The following form of those equations is mostly used

$$P_{W_j} = \ell_j f^3 D^4 \,\mathrm{fnc}\left(\frac{A_j}{D}\right), \tag{5.2}$$

where $\mathrm{fnc}(A_j/D)$ is the reduced power function (function of relative vibration amplitude A_j/D), A_j is the local vibration amplitude inside the jth sub-span, f is vibration frequency and ℓ_j is the sub-span length [10]. Power dissipated due to conductor self-damping is estimated using the empirical estimation [5, 19, 25]

$$P_{C_j} = \ell_j K \frac{\left(\frac{A_j}{D}\right)^l f^m}{T^n}, \tag{5.3}$$

where K is the so-called proportionality factor that characterizes the self-damping properties of each conductor, and l, m and n are the exponents of the amplitude, frequency and conductor tension. The exponents l, m and n, according to Claren & Diana [5] are used in this paper. The proportionality factor K is determined according to data from [3].

The power dissipated in the damper is calculated using the equation given in [26]

$$P_{D_j} = \frac{1}{2}\,\mathrm{Re}(s^2 W_{D_j}^* Z_{D_j}^* W_{D_j}), \tag{5.4}$$

where $Z_{D_j}^*$ is the complex impedance of the jth damper, W_{D_j} is the complex amplitude of the jth damper clamp and $*$ denotes complex conjugation. The Stockbridge vibration damper impedance is usually determined by a procedure [14] which takes into account only the translational motion of the damper for vibration velocity amplitude of 100 mm/s.

Although the cable bending stiffness is small and does not significantly impact the resonant frequencies, it is necessary to know its value to determine the cable bending strain ε. The general expression for bending strain is

$$\varepsilon(x,t) = \frac{d}{2} w''(x,t), \tag{5.5}$$

where d is empirically determined bending diameter which is not equal to the cable diameter D due to the cable's complex structure. In this paper we use the expression (given in [12, 26]) for bending strain

$$\varepsilon \approx \frac{w'_{\mathrm{eff}}}{\ell_{\mathrm{char}}} \cdot \frac{d}{2}, \quad \ell_{\mathrm{char}} = \sqrt{\frac{EI}{T}}, \tag{5.6}$$

where ℓ_{char} is the "characteristic cable length" and w'_{eff} is the effective slope of the cable at the suspension clamps, damper clamps and warning sphere clamps [9, 26].

6. Numerical results

The numerical computation was done in Matlab, since it has many built-in linear algebra functions (based on LAPACK) that enable fast numerical computation. Besides the built-in functions for the SVD, we also have used two optimization functions, `fsolve` with the Levenberg–Marquardt algorithm option, and `fminsearch` with the different values of the termination tolerances `TolFun` (the function value tolerance) and `TolX` (the termination tolerance for the independent variable). Both procedures use default number of iterations and function evaluations.

We have used the function `svd` that computes the SVD all the singular values instead of the `svds`, which is designed to find only a few of them. When `svds` is used to find only the minimal singular value, it sometimes fails (when $J(s)$ is nearly singular) with a report that the singular value of a 0×1 rectangular matrix is requested.

We have also tried to compute the full SVD of $J(s)$ (with the left and the right singular vectors) with intention to preprocess the matrix obtained in the next optimization step (for new s), but this approach did not speed up the computation of singular values.

The presented test-results are related to Aluminium Conductor Steel Reinforced (ACSR) "Bersfort" 35.6 mm (48/7) with four Stockbridge dampers and two warning spheres, as shown in Fig. 4.2 (d = 22.2 mm, ρA = 2.37 kg/m, EI = 2105 Nm^2, P = 180.1 kN, T/P = 0.22, m = 12.36 kg, J_C = 1.79 kg m^2, l_{St} = 0.9 m).

In the following discussion it is illustrated a) that the NSS (Nonhomogeneous System Solution) method is not accurate and b) that it does not yield physically possible results. Fig. 6.1 (a) shows absolute values of cable bending strains $|\varepsilon_L|$ at the left, and $|\varepsilon_R|$ at the right suspension clamp, obtained by the NSS method, also called alternate approach in [26–28], for the default values of optimization parameters (`TolX` = 10^{-6}, `TolFun` = 10^{-6}).

(a)

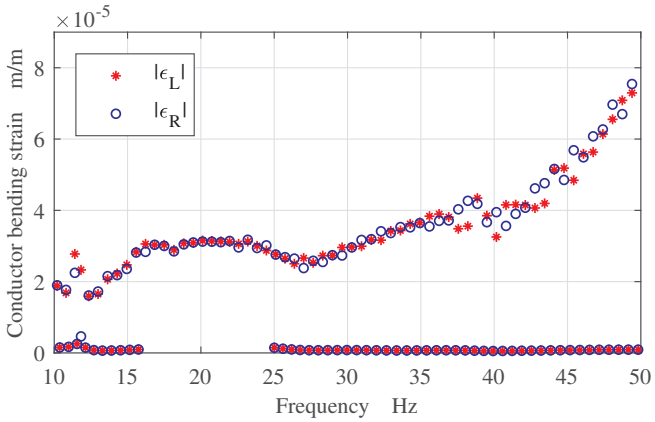

(b)

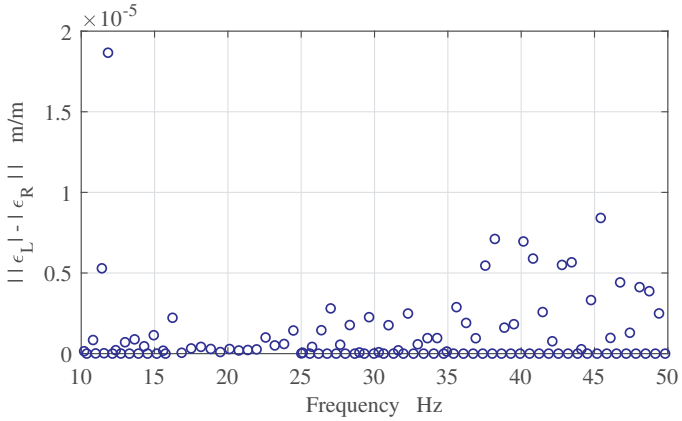

Figure 6.1: (a) Absolute values of cable bending strains at the left and the right suspension clamp, (b) $||\varepsilon_L| - |\varepsilon_R||$, obtained by the NSS method.

As one can see, at most frequencies, $|\varepsilon_L|$ and $|\varepsilon_R|$ are the same (the circles and asterisks overlap). However, at some frequencies different values for $|\varepsilon_L|$ and $|\varepsilon_R|$ are obtained. These differences can be easily seen in Fig. 6.1 (b) that shows $||\varepsilon_L| - |\varepsilon_R||$.

Fig. 6.2 shows cable mode shapes, in terms of the absolute values of relative vibration amplitudes A/D for two natural frequencies, f = 10.2 Hz and f = 11.41 Hz. The mode shape shown in Fig. 6.2 (a) is symmetrical while the mode shape shown in Fig. 6.2 (b) is asymmetrical.

These results indicate an error in the procedure of determination of the system matrix eigenvalues because mode shapes of symmetrical structures (Fig. 4.2) must be either symmetric or antisymmetric (they cannot be asymmetric).

As it is explained in Section 4.1, if the NSS method is used, it is not immediately clear (without additional SVD, QR, or other check of singularity) whether the obtained solution is the system matrix eigenvalue or only one of the local minima of the function $\sigma_{\min}(J(\omega, \delta))$. Fig. 6.3 shows $|\varepsilon_L|$ and $|\varepsilon_R|$ obtained by the SVD, and the hybrid optimization method `SVD_OPT` for `TolX` = 10^{-8}, `TolFun` = 10^{-12} for the Levenberg–Marquardt method, and `TolX` = `TolFun` = 10^{-14} for the Nelder–Mead search method.

These results differ significantly from the results obtained by the NSS method (Fig. 6.1). The contribution of the Nelder–Mead direct search method can be easily observed in Fig. 6.4.

(a)

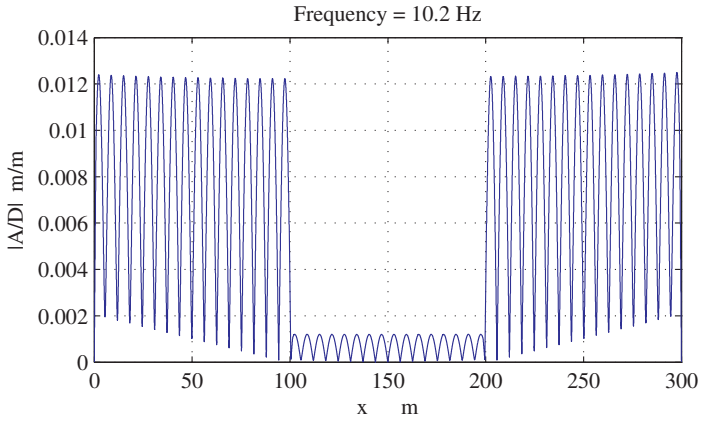

(b)

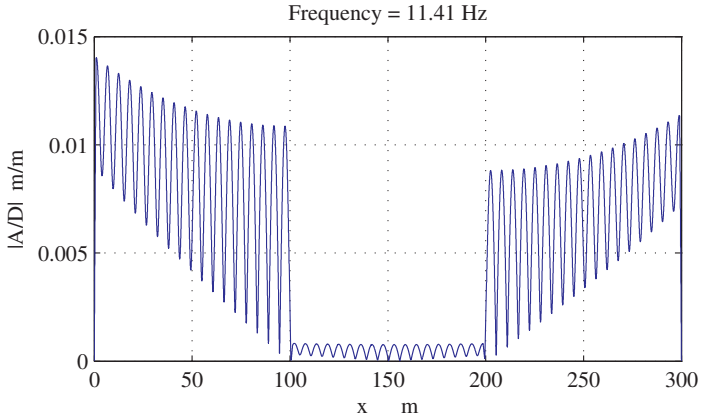

Figure 6.2: Cable mode shapes (absolute values of relative vibration amplitudes A/D), (a) symmetric, (b) asymmetric, obtained by the NSS method.

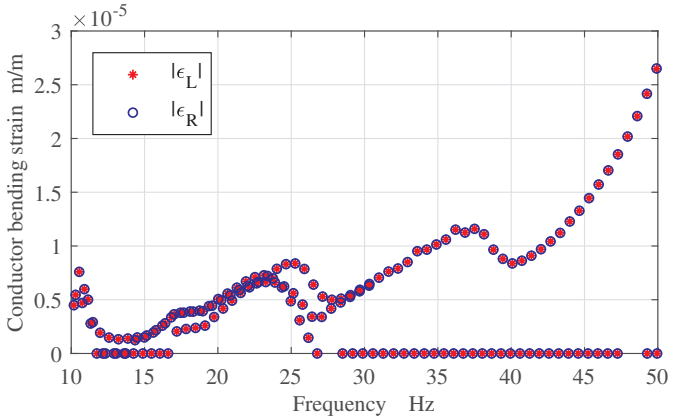

Figure 6.3: Absolute values of cable bending strains at the left and the right suspension clamp obtained by the `SVD_OPT` method.

The comparison of results obtained by the NSS method (Fig. 6.1 (a)) and the `SVD_OPT` method (Fig. 6.3) is shown in Fig. 6.5.

(a)

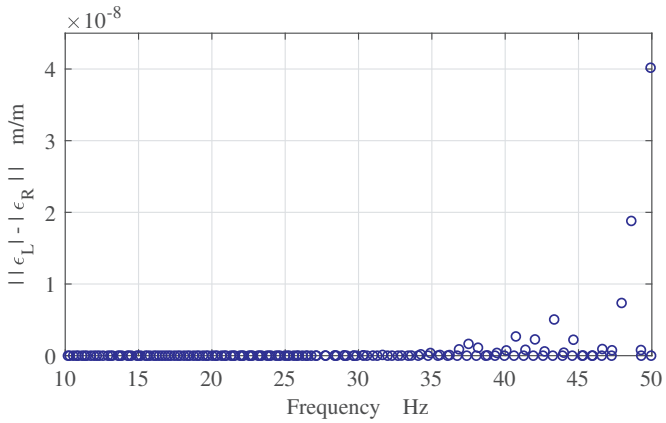

(b)

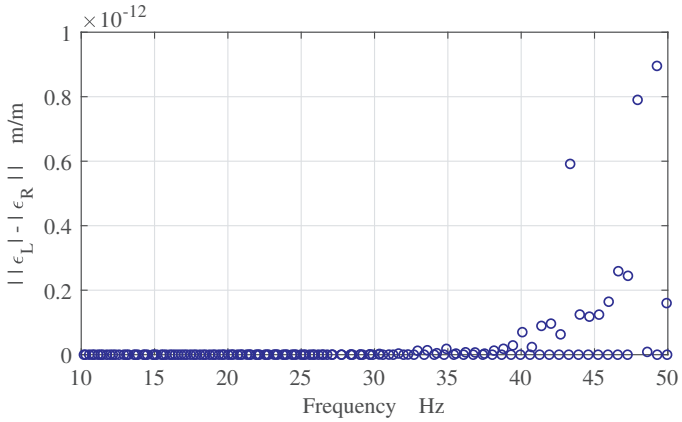

Figure 6.4: $||\varepsilon_L| - |\varepsilon_R||$ obtained (a) by the procedure that uses only the Levenberg–Marquardt method, (b) by the procedure that additionally uses the Nelder–Mead direct search method.

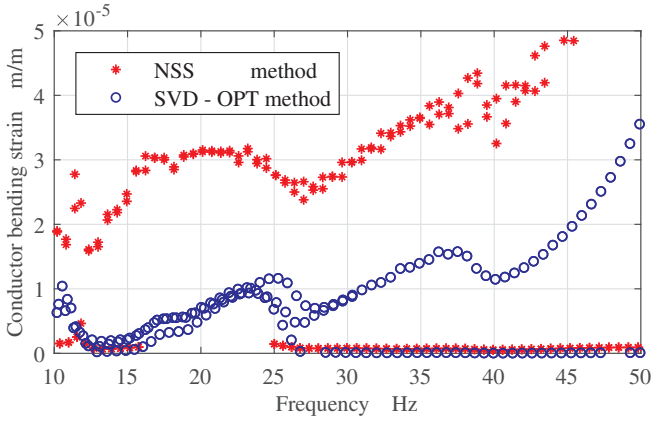

Figure 6.5: Comparison of results obtained by the NSS method and the `SVD_OPT` method.

As one can see, there are large differences among strains determined by the NSS and the `SVD_OPT` (within a large area of frequencies strains determined by the NSS are several times greater than those obtained by the `SVD_OPT`).

The reason for this lay in inadequately precisely determined eigenvalues of the system matrix $J(s)$, i.e., in mode shapes obtained by the NSS, which are physically not possible for a symmetrical structure (Fig. 4.2).

In the example considered, results obtained by both methods (the procedure that uses only the Levenberg–Marquardt method, (Fig. 6.4 (a), `TolX` = 10^{-8}, `TolFun` = 10^{-12}) and the procedure that additionally uses the Nelder–Mead direct search method (Fig. 6.4 (b), `TolX` = `TolFun` = 10^{-14}, `cln_fct` = 10^{-4}) are similar in shape. Note that $||\varepsilon_L| - |\varepsilon_R||$ in Fig. 6.4 (a) is of order 10^{-7}, but only of order 10^{-11} in Fig. 6.4 (b).

Fig. 6.6 shows the minimal singular values of the system matrix $J(s)$. If the computed singular value is under the threshold limit `cln_fct`, parameter s is accepted as the parameter that makes $J(s)$ singular. The value of the parameter `cln_fct` is determined by extensive testing—the usual bound for `cln_fct` (condition number of $J(s)$ times the machine epsilon) is useless here, since in each step, the optimization method makes the matrix more singular.

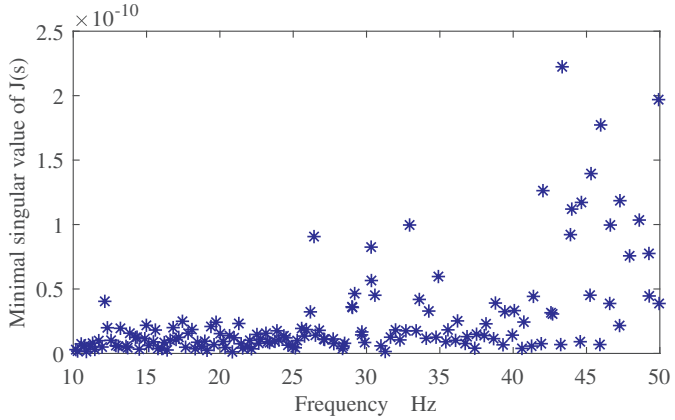

Figure 6.6: Minimal singular values of $J(s)$.

Finally, note that when the dimensions of matrices $J(s)$ are growing, the maximal singular values of the initial matrices for optimization $\sigma_{\max}(J(\omega, \delta'))$ are also growing. Since the condition number i.e., $\sigma_{\max}(J(\omega, \delta'))/\sigma_{\min}(J(\omega, \delta'))$ is directly linked to the accuracy of the computed minimal singular value—the minimal singular value for larger $J(s)$ are even harder to find accurately.

7. Conclusion

In this paper we have proved that the rank of a system matrix $J(s)$ of a transmission line cable with in line fittings (Stockbridge type vibration dampers and warning spheres) is either full, or full rank minus one. Therefore, since eigenvalue zero is single, convergence of a numerical procedure for its determination is usually faster than the determination of a multiple eigenvalue. We have also developed a numerical procedure that searches for parameters s that makes the matrix $J(s)$ singular. The numerical procedure, which is easily parallelizable, consists of the hybrid minimization method paired with the SVD for the detection of the singularity of the matrix $J(s)$. Obtained numerical results for the symmetrical structures show that the corresponding mode shapes are, as expected, either symmetric or antisymmetric.

Precise determination of the parameter s is crucial for reliable application of Modified Energy Balance Method using eigenfunctions, which is usually used for overhead transmission line with in-span fittings Aeolian vibration response determination and fatigue life assessment.

Since the same numerical problems that are described in this work occur in determination of system eigenvalues of bundled conductors with in line spacer dampers the developed numerical procedure can also be very useful when MEBM is used to determine the Aeolian vibration response of bundled conductors. The block structure of the matrix $J(s)$ for a single transmission line and $J(s)$ for the bundle is the same. In the case of a bundle the dimensions of inner blocks of $J(s)$ are larger, and its inner structure is more complicated. Our testing routines for bundles that consist of 2–4 subconductors show that the method developed here works very well even in these cases.

Acknowledgements

This work has been supported in part by Croatian Science Foundation under the project IP-2014-09-3670. This project has received funding from the European Union's Horizon 2020 research and innovation programme under the Marie Sklodowska–Curie grant agreement no. 657539 STARMAS.

References

[1] C. R. F. Azevedo, A. M. D. Henriques, A. R. P. Filho, J. L. A. Ferreira, J. A. Araújo, Fretting fatigue in overhead conductors: Rig design and failure analysis of a Grosbeak aluminium cable steel reinforced conductor, Eng. Fail. Anal. 16 (2009) 136–151.
[2] C. A. Bavastri, J. J. Espíndola, P. H. Teixeira, A hybrid algorithm to compute the optimal parameters of a system of viscoelastic vibration neutralisers in a frequency band, in: Proceedings of MOVIC'98, Zürich, Switzerland, 1998, pp. 577–582.
[3] CIGRE TF 22.11.1, Modeling of Aeolian vibration of single conductors: Assessment of the technology, Appendix A, Electra 181 (1998).
[4] CIGRE TF B2.11.01, Modelling of Aeolian vibrations of a single conductor plus damper: Assessment of technology, Electra 223 (2005) 28–36.
[5] R. Claren, G. Diana, Dynamic strain distribution on loaded stranded cables, IEEE T. Power Ap. Syst. PAS-88 (11) (1969) 1678–1690.
[6] R. Claren, G. Diana, Mathematical analysis of transmission line vibration, IEEE T. Power Ap. Syst. PAS-88 (12) (1969) 1741–1771.
[7] R. Claren, G. Diana, F. Giordana, E. Massa, Vibrations of transmission line conductor bundles, IEEE T. Power Ap. Syst. PAS-90 (4) (1971) 1796–1814.
[8] A. A. Fadel, D. Rosa, L. B. Murça, J. L. A. Fereira, J. A. Araújo, Effect of high mean tensile stress on the fretting fatigue life of an Ibis steel reinforced aluminium conductor, Int. J. Fatigue 42 (2012) 24–34.
[9] P. Hagedorn, Ein einfaches Rechenmodell zur Berechnung winderregter Schwingungen an Hochspannungsleitungen mit Dämpfern, Ing. Arch. 49 (3–4) (1980) 161–177.
[10] P. Hagedorn, On the computation of damped wind–excited vibrations of overhead transmission lines, J. Sound Vib. 83 (2) (1982) 253–271.
[11] P. Hagedorn, Wind–excited vibrations of transmission lines: A comparison of different mathematical models, Math. Mod. 8 (1987) 352–358.
[12] P. Hagedorn, N. Mitra, T. Hadulla, Vortex–excited vibrations in bundled conductors: A mathematical model, J. Fluid. Struct. 16 (7) (2002) 843–854.
[13] N. J. Higham, Accuracy and Stability of Numerical Algorithms, 2nd ed., SIAM, Philadelphia, 2002.
[14] IEC-61897, Overhead lines – requirements and tests for Stockbridge type Aeolian vibration dampers, Commission Electrotechnique Internationale, International Standard (1998) 25–33.
[15] M. Kraus, P. Hagedorn, Aeolian vibrations: Wind energy input evaluated from measurements on an energized transmission line, IEEE T. Power Deliver. 6 (3) (1991) 1264–1270.
[16] K. Levenberg, A method for the solution of certain non-linear problems in least squares, Quart. Appl. Math. 2 (1944) 164–168.
[17] M. Markiewicz, Optimum dynamic characteristics of stockbridge dampers for dead-end spans, J. Sound Vib. 188 (2) (1995) 243–256.
[18] D. Marquardt, An algorithm for least-squares estimation of nonlinear parameters, SIAM J. Appl. Math. 11 (2) (1963) 431–441.
[19] S. Meynen, H. Verma, P. Hagedorn, M. Schafer, On the numerical simulation of vortex-induced vibrations of oscillating conductors, J. Fluid. Struct. 21 (2005) 41–48.
[20] J. A. Nelder, R. Mead, A simplex method for function minimization, Comput. J. 7 (1965) 308–313.
[21] V. Novaković, A hierarchically blocked Jacobi SVD algorithm for single and multiple graphics processing units, SIAM J. Sci. Comput. 37 (2015) C1–C30.
[22] A. Simpson, N. J. Salmon, C. N. Taylor, Computational comparison of efficacies of Aeolian vibration damping devices for multiconductor overhead power–lines, IEE Proc.–C 137 (3) (1990) 225–232.
[23] S. Singer, S. Singer, V. Novaković, D. Davidović, K. Bokulić, A. Uščumlić, Three-level parallel *J*-Jacobi algorithms for Hermitian matrices, Appl. Math. Comput. 218 (2012) 5704–5725.
[24] S. Singer, S. Singer, V. Novaković, A. Uščumlić, V. Dunjko, Novel modifications of parallel Jacobi algorithms, Numer. Alg. 59 (2012) 1–27.
[25] J. Vecchiarelli, I. G. Currie, D. G. Havard, Computational analysis of Aeolian conductor vibration with a Stockbridge-type damper, J. Fluid. Struct. 14 (2000) 489–509.
[26] H. Verma, Aerodynamic and structural modeling for vortex-excited vibrations in bundled conductors, Ph.D. thesis, Technische Universität Darmstadt (2008).
[27] H. Verma, P. Hagedorn, Wind induced vibrations of long electrical overhead transmission line spans: A modified approach, Wind Struct. 8 (2) (2005) 89–106.
[28] H. Verma, P. Hagedorn, Different numerical techniques for the solution of transcedental eigenvalue problem in transmission line bundles, ANZIAM J. 47 (2007) C873–C893.
[29] C. H. K. Williamson, R. Govardhan, A brief review of recent results in vortex-induced vibrations, J. Wind Eng. Ind. Aerod. 96 (2008) 713–735.